The impact of hydrograph variability and frequency on sediment transport dynamics in a gravel-bed flume

Plumb, Ben D.; Juez, Carmelo; Annable, William K.; McKie, Chris W.; Franca, Mario J.

DOI
10.1002/esp.4770

Publication date
2019

Document Version
Final published version

Published in
Earth Surface Processes and Landforms

EARTH SURFACE PROCESSES AND LANDFORMS
Earth Surf. Process. Landforms **45**, 816–830 (2020)

Published online 12 December 2019 in Wiley Online Library
(wileyonlinelibrary.com) DOI: 10.1002/esp.4770

The impact of hydrograph variability and frequency on sediment transport dynamics in a gravel-bed flume

Ben D. Plumb,[1] Carmelo Juez,[2,3,4]* William K. Annable,[1] Chris W. McKie[1] and Mario J. Franca[2,5]
[1] Department of Civil and Environmental Engineering, University of Waterloo, Waterloo, Ontario Canada
[2] Laboratoire de Constructions Hydrauliques, École Polytechnique Fédérale de Lausanne, Lausanne, Switzerland
[3] Fluid Mechanics Department, ETSIDI, Universidad Politécnica de Madrid, Madrid, Spain
[4] Instituto Pirenaico de Ecología, Consejo Superior de Investigaciones Científicas (IPE-CSIC), Campus de Aula Dei, Zaragoza, Spain
[5] Water Science and Engineering department, IHE – Delft Institute for Water Education and Department of Hydraulic Engineering, Delft University of Technology, Delft, Netherlands

Received 2 May 2019; Revised 11 November 2019; Accepted 13 November 2019

*Correspondence to: Carmelo Juez, Instituto Pirenaico de Ecología, Consejo Superior de Investigaciones Científicas (IPE-CSIC), Campus de Aula Dei, Zaragoza, Spain.
E-mail: carmelo.juez@ipe.csic.es

ESPL
Earth Surface Processes and Landforms

ABSTRACT: A laboratory study was undertaken to investigate how changes in flow regime and hydrograph shape (number of cycled hydrographs and duration of each hydrograph) together impact bedload transport and resulting bed morphology. Three hydrologic conditions (experiments) representing different levels of urbanization, or analogously different flow regimes, were derived from measured hydrometric field data. Each experiment consisted of a series of hydrographs with equal peak discharge and varying frequency, duration and flashiness. Bedload transport was measured throughout each hydrograph and measurements of bed topography and surface texture were recorded after each hydrograph. The results revealed hysteresis loops in both the total and fractional transport, with more pronounced loops for longer duration hydrographs, corresponding to lower rate of unsteadiness until reaching the peak discharge (pre-urbanization conditions). Shorter duration hydrographs (urban conditions) displayed more time above critical shear stress thresholds leading to higher bedload transport rates and ultimately to more variable hysteresis patterns. Surface textures from photographic methods revealed surface armoring in all experiments, with larger armor ratios for longer duration hydrographs, speculated to be due to vertical sorting and more time for bed rearrangements to occur. The direction of bed surface adjustment was linked to bedload hysteresis, more precisely with clockwise hysteresis (longer hydrographs) typically resulting in bed coarsening. More frequent and shorter duration hydrographs result in greater relative channel adjustments in slope, topographic variability and surface texture. © 2019 John Wiley & Sons, Ltd.

KEYWORDS: sediment transport; river morphology; urbanization; hydromodification; bedload hysteresis; unsteady flow; cycled hydrograph

1. Introduction

The adjustment of channel form in a gravel-bed channel is concordant with the magnitude and frequency of discharges capable of transporting bed material (Wolman and Miller, 1960; Poff et al., 1997). Although it is common to characterize fluvial changes by a single discharge (Leopold *et al.*, 1964), a channel is ultimately formed by the range in competent flows capable of performing work on the erodible boundaries (Lenzi et al., 2006; Surian et al., 2009; Plumb et al., 2017). These competent flows, combined with the amount and sizes of transported sediment, interact with the bed and banks to determine an equilibrium condition in terms of hydraulic resistance and amount of sediment transported. When this magnitude and frequency relationship (the natural flow regime) is altered, the channel morphology will adjust to the new boundary conditions (e.g. Lane, 1955; Schumm *et al.*, 1987).

The natural flow regime has been characterized by five components; magnitude, frequency, duration, timing and flashiness or unsteadiness (Poff et al., 1997). Although this characterization was based upon processes that regulate the ecological integrity of a watercourse, these five metrics also influence sediment transport and the resulting morphology of a channel. Flow regimes can be altered due to many anthropogenic activities such as dam construction, water diversions for irrigation, land-use changes such as deforestation, forest fires and urbanization or levee construction and channelization. These alterations can result in different impacts to the flow regime (Poff et al., 1997) that have varying impacts on channel morphology (Gregory, 2006; Bombar et al., 2011).

Among the five components that characterize the natural flow regime, this study focuses on unsteadiness. In nature, flows that transport sediment and perform geomorphic work can be steady (constant discharge) or unsteady (discharge fluctuates in rising and falling limbs driven by climate forcing such as snowmelt or rainfall). Unsteady flow and associated bedload are known to produce hysteresis, i.e. a lag between discharge and bedload transport rates (Gunsolus and Binns, 2017). The mechanistic interpretation of this phenomenon is the modulation of the sediment yields due to the fluctuation of the hydraulic forces exerted on the riverbed (Gunsolus and Binns, 2017) and due to the origin of sediments (proximal or distal availability of sediments) (Juez et al., 2018; Matos et al., 2018). Common classes of sediment hysteresis are (1) clockwise, indicating a greater sediment transport rate on the rising limb of hydrographs; (2) counterclockwise, indicating a greater sediment transport rate on the falling limb of hydrographs; (3) single value plus a loop, a combination of 1 and either 2 or 3; and (4) figure eight, a combination of 2 and 3. Although these classes were originally characterized for suspended sediment concentrations and discharge relations (Williams, 1989), they have also been observed for bedload transport under unsteady flow conditions in both field (Reid et al., 1985; Sidle, 1988; Kuhnle, 1992; Hassan and Church, 2001) and laboratory studies (Lee et al., 2004; Mao, 2012; Humphries et al., 2012; Waters and Curran, 2015; Wang et al., 2015; Mrokowska *et al*., 2016; Mrokowska and Rowinski, 2019). Clockwise hysteresis has been attributed to 'a lag in the formation' of roughness elements to arrest sediment transport (Kuhnle, 1992) or to an initially loose bed due to antecedent floods (Reid et al., 1985). Counterclockwise hysteresis is commonly attributed to bedform lag (Lee et al., 2004) as well as bed stabilization due to antecedent periods of low flow (Reid et al., 1985; Waters and Curran, 2015).

Bedload hysteresis and surface grain size hysteresis (also known as fractional transport hysteresis or bedload percentiles) have been documented in laboratory settings. Hassan et al. (2006) reported gradual coarsening and fining of bedload during rising and falling limbs of experiments, respectively, indicative of clockwise hysteresis of the grain sizes. Bed surface textures for hydrographs of shorter duration did not change considerably, attributed to less time for winnowing or settling processes to occur due to the short durations of the hydrographs (Hassan et al., 2006). When longer duration hydrographs were studied, channel beds showed a gradual coarsening during the falling limbs of experiments, indicating that sufficient time for particle winnowing and settling had been achieved (Hassan et al., 2006). Similar surface texture trends were obtained by Mao (2012), with hydrographs corresponding to lower peak discharges showing greater degrees of bed coarsening on falling limbs. Bedload percentiles, however, exhibited a counterclockwise trend, with coarser bedload observed on the falling limb (Mao, 2012). Conversely, Wang et al. (2015) reported bed surface fining for hydrographs with a shorter rising limb and bimodal sediments, and little change in bed surface texture for hydrographs with a longer rising limb for both unimodal and bimodal sediment mixtures.

Antecedent low-flow conditions prior to unsteady flow hydrographs has been shown to increase bed stability (Reid et al., 1985; Mao, 2012; Waters and Curran, 2015); however, the impact of hydrograph frequency on bedload transport dynamics has been less documented at the laboratory scale. Ferrer-Boix and Hassan (2015) documented a systematic decrease in bedload transport rates due to more frequent flood pulses and attributed it to interrelated sediment storage and downstream fining. More recently, several studies (Mao, 2018; Phillips et al., 2018; Redolfi et al., 2018; Bakker et al., 2019) have initiated the investigation on the impact of flood hydrographs on bedload transport dynamics.

These experiments illustrate the importance of unsteady hydrograph parameters (shape, flashiness, duration and frequency) on sediment transport and the resulting bed morphology, yet the exact influence of hydrograph characteristics on sediment transport and bed morphology remains largely unknown, as recent studies point out (Gunsolus and Binns, 2017; Phillips et al., 2018). Moreover, little work has been done to date that combines changes in hydrograph shape and frequency to investigate sediment transport dynamics. An understanding of sediment transport characteristics of both the existing and desired outcomes is a fundamental component of stream rehabilitation projects (Shields et al., 2003). Given that stream restoration projects are becoming increasingly common (Bernhardt *et al*., 2005), it is necessary to further our understanding on how changes in flow regime impact sediment transport and resulting bed morphology.

Here we investigate the questions of how common changes in the flow regime (frequency) and unsteady flows (duration) together impact bedload transport rates and sediment sizes, bedload hysteresis, bed surface textures and bed topographic variability. To address these questions, a series of unsteady flow laboratory experiments were designed to represent different flow regimes. We use a field example related to watershed urbanization where the experiments were designed to represent different stages of watershed urbanization, ranging from rural (non-urban land use) to highly urbanized. Hydrograph parameters (flashiness and duration) and average annual frequency of events corresponding to a specific return period were derived from hydrometric gauge stations of two urbanizing watersheds, collectively spanning the entire land-use transformation from rural to urban, encompassing varied flow regimes. Specific objectives of this study were to characterize the bedload transport responses (rates, yields, sizes and hysteresis) to differing hydrographs as well as investigate how differing hydrograph characteristics impact the resulting bed texture and topographic variability. The experimental channel conditions are inspired by field data (Plumb et al., 2017); however, the general nature of the experiments allow for more general interpretations towards the impacts of flow regime and unsteady flows on sediment dynamics in gravel-bed channels.

2. Methods

2.1. Experimental design

Three experiments were conducted, representing three different flow regimes derived from hydrometric data from urbanizing rivers in Southern Ontario, Canada (Plumb et al., 2017). Specific details regarding the design of the hydrograph parameters are discussed later in this section. Hydraulic and sediment properties are roughly scaled to one of the rivers used to derive the hydrologic data, Mimico Creek (a scale of 1:24). A poorly sorted bimodal sand–gravel mixture with bulk material characteristics for $D_{30\text{bulk}}$, $D_{50\text{bulk}}$, $D_{84\text{bulk}}$, $D_{90\text{bulk}}$ and D_{maxbulk} of 0.5 mm, 2 mm, 6.5 mm, 7 mm and 10 mm, respectively, were used. For each experiment, peak discharge was held constant and only time to peak, duration and frequency were altered. Excess shear (ratio of applied shear stress and critical shear stress: τ_0/τ_c) for the hydrographs ranges between 1.7–2.9 and 1–1.8 for the $D_{50\text{bulk}}$ and $D_{84\text{bulk}}$ particle sizes, respectively. Each triangular hydrograph was approximated in a series of short steps, as has been done in previous experiments simulating unsteady flow (Hassan et al., 2006; Mao, 2012; Martin and Jerolmack, 2013; Waters and Curran, 2015). The Froude number in the experiments ranged from 0.4 to 0.8 (estimated based on measured flow depths and known discharges), which is within range of the prototype streams and previous experiments studying unsteady flow (Lee et al., 2004; Mao, 2012; Waters and Curran, 2015). Peak sediment input rates were established based on measured bedload transport rates in Mimico Creek and scaled to the flume by means of Froude similarity; see Annable et al. (2012) and Plumb et al. (2017) for details on field sampling methods and results. The sediment input rating curve was approximated into two input rates, such that the input rate was increased partway through the rising limb, at 70% of the peak discharge (Q_{peak}) and then decreased part way through the falling limb. This two-step sediment input was done to simplify the experimental procedure as the sediment input rate required manual adjustment. The difference in total sediment input using this two-step method and adjusting during every discharge step was less than 5%, confirmed through computation of the total load transported using the scaled bedload rating curve and the two-step method. A summary of the experimental boundary conditions is provided in Table I.

Also shown in Table I, there is an unsteadiness parameter, which has been previously derived to characterize sediment yield in unsteady flow hydrographs. The total flow work index (W_k) (Yen and Lee, 1995) represents the total work performed by the hydrograph:

$$W_k = \frac{u_{*0}^2 V_h}{g {h_0}^3 B} \# \quad (1)$$

<N>where u_{*0} is the shear velocity at base flow and calculated assuming quasi-uniform conditions (as $\sqrt{\tau_0/\rho}$ at the low point of the hydrograph, τ_0 is applied shear stress and ρ is density of water), V_h is the hydrograph volume, h_0 is the flow depth at base flow (taken at the low point of the hydrograph), B is the channel width and g is the acceleration due to gravity.

2.2. Experimental channel and measurements

Experiments were conducted at the Laboratoire de Constructions Hydrauliques (LCH), at the École Polytechnique Fédérale de Lausanne (EPFL), using a 9 m long × 0.5 m wide flume, with sediment being supplied at the upstream end by an Archimedes screw sediment feeder (Figure 1). A calibrated valve–discharge relationship, which was tested to be ±10% accurate for each discharge step, was used to simulate the experimental hydrographs. Discharge was continuously measured at the channel inlet using a V-notch weir and ultrasonic sensor. Bedload transport was measured by a bedload trap located at the downstream end of the flume, where the sediment was routed through a valve and into a 0.125 mm collection bin, which was emptied between each discharge step, such that individual rates and textures could be obtained throughout the rising limb, peak and falling limb of each hydrograph (Figure 1). Sediment samples were subsequently dried, weighed and sieved at the half-phi scale.

Throughout each hydrograph, flow depth was continuously measured using a series of ultrasonic sensors placed throughout the channel, and verified by measurements with a ruler against the clear channel walls. After each hydrograph, topographic scans were conducted using a mini echo sounder, with an accuracy of ±1 mm, along a 3.5 m long reach of the channel at the downstream end. This 3.5 m long reach was chosen at the downstream end to ensure that the sediment transport rates and resulting bed texture were not influenced by the upstream boundary conditions of the channel (i.e. the sediment feeder). The exact distance between the sediment feeder and the reach of study, 5.0 m, is equal to 10 times the channel width, and is a common practice for guaranteeing the independence of the boundary conditions (Guillén-Ludeña et al., 2015; Ferrer-Boix *et al.*, 2015). No bed discordance or aggradational wedge

Table I. Experimental hydrograph variables derived from gauge data and associated unsteady flow parameters

Scenario	Q_{thres} (L s^{-1} m^{-1})	q_{peak} (L s^{-1} m^{-1})	$q_{s,in}$ (low) (g s^{-1} m^{-1})	$q_{s,in}$ (high) (g s^{-1} m^{-1})	TTP (min)	t_h (min)	V_h (m^3)	Frequency (# yr^{-1})[a]	No. hyd.	t_{tot} (h)	V_{tot} (m^3)	W_k	τ_{thres} (N/m^2)	τ_{peak} (N/m^2)	$\tau_{c30bulk}$ (N/m^2)	$\tau_{c50bulk}$ (N/m^2)	$\tau_{c90bulk}$ (N/m^2)
LU1	12.0	32.0	8.0	14.0	42.0	82.0	52.0	0.9	9.0	12.3	468.0	748.0	2.5	4.2	0.5	1.5	4.4
LU2	12.0	32.0	8.0	14.0	21.0	45.0	28.5	1.6	16.0	12.0	456.0	409.9	2.5	4.2	0.5	1.5	4.4
LU3	12.0	32.0	8.0	14.0	21.0	37.0	23.5	3.3	33.0	20.4	775.5	338.0	2.5	4.2	0.5	1.5	4.4

Note: Three land-use scenarios were established (LU1, LU2 and LU3), each representing a different range of urban land-use and used to define the three experiments conducted here (further details in Table II). q_{thres} is threshold discharge, q_{peak} is peak discharge, $q_{s,in}$ is sediment input rate, TTP is time-to-peak, t_h is hydrograph duration, V_h is hydrograph volume, t_{tot} is total experimental time, V_{tot} is total volume of water, W_k is total flow work index for each hydrograph, τ_{thres} is the applied shear stress at the threshold discharge, τ_{peak} is the applied shear stress at peak discharge, and $\tau_{c30bulk}$, $\tau_{c50bulk}$ and $\tau_{c90bulk}$ are the critical shear stresses for D_{30bulk}, D_{50bulk} and D_{90bulk}, respectively.
[a]The frequency of the hydrographs per year was derived from hydrometric time series described in Plumb et al. (2017).

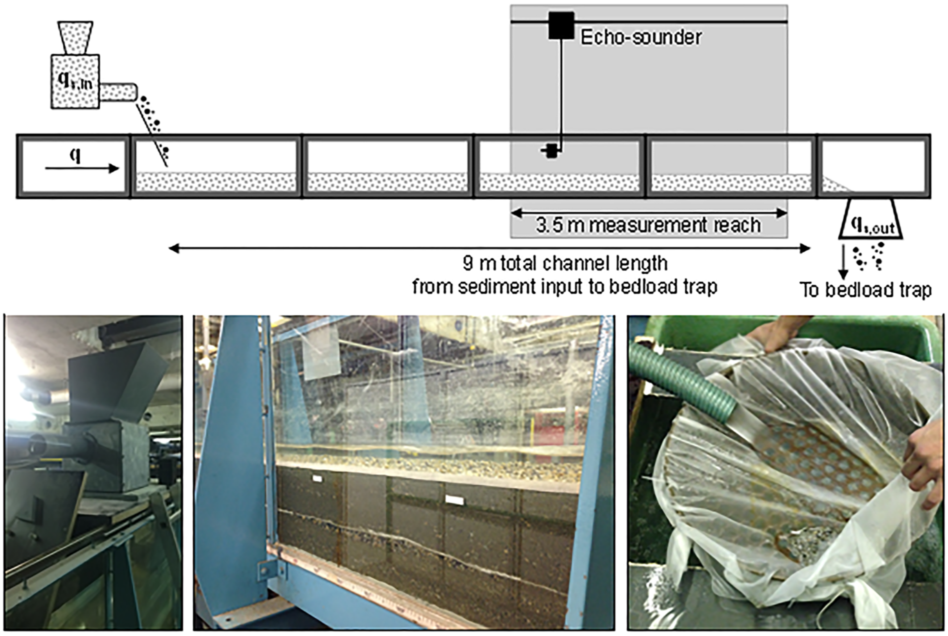

Figure 1. Schematic of experimental channel (top) and photos illustrating the sediment feeder (left), the channel during experiments (middle) and the downstream sediment trap (right). [Colour figure can be viewed at wileyonlinelibrary.com]

was observed in the channel before and after the reach of study. Accordingly, we assume the sediment supply was well fed in the channel. A series of 20 longitudinal profiles spaced every 0.02 m along the channel width were conducted after each hydrograph with the echo sounder, obtaining measurements every 0.01 m in the stream-wise direction. Due to physical limitations of the instrument, 0.06 m closest to the sidewalls could not be scanned. The grain size distribution (GSD) of the bed was also obtained in this 3.5 m measurement reach using high-resolution (12 MP) photos. Similar to methods used by Mao (2012), a 0.3 m × 0.3 m grid was imposed over each photo using CAD software. The *b*-axis (intermediate axis) was digitized for the 64 particles located at each node of the grid (grid spacing of 4.3 cm), resulting in up to 768 particles for each GSD estimate. It should be noted that some photos (<3% of total) and nodes (<1% of total) were not suitable for the analysis due to lighting and/or blurriness. These photos and nodes were subsequently removed from the analysis.

2.3. Hydrologic scenario setup

Hydrological inputs for the laboratory experiments were designed based upon combining the temporal land-use trends of two urbanizing rivers located in Toronto, Ontario, Canada: Etobicoke Creek (67.7 km^2) and Mimico Creek (73.8 km^2); see Plumb et al. (2017) for further discussion on the paired watershed space-for-time substitution. Both watersheds have approximately 45 years of instantaneous (15 min) discharge data, with similar watershed areas (<10% difference), channel morphologies and, due to their proximity, similar rainfall (Annable et al., 2012; Thompson, 2013). Their principal physical difference is the amount of land-use change that has occurred in the period of record, verified by temporal aerial photo analysis (Thompson, 2013). Etobicoke Creek has evolved from rural to 20% urban land use, while Mimico Creek has transformed from 45% to 88% urban land use during the same period of hydrometric record. A space-for-time substitution was undertaken with the objective of combining the time series stream gauge data for both watersheds to construct an approximate 60-year hydrologic record representing the evolution of a watershed ranging from rural (~0% urban land-use) to nearly fully urbanized. From this series, three land-use scenarios were established, each representing a different range of urban land use and used to define the three experiments conducted here (Table II).

The 1-year return period discharge of the pre-development prototype (Thompson, 2013) watershed was chosen to capture the change in intermediate, competent discharge events due to urbanization, which have been shown to change more than larger magnitude events (Hollis, 1975; Booth, 1990; Annable *et al.*, 2010). Hydrographs with peak discharges falling within a ±10% range of this discharge were used to populate the event database for each land-use scenario investigated.

For each hydrograph (approximating the 1-year return period discharge of the pre-development scenario) total volume, total time to peak, total duration, threshold volume, threshold time to peak and threshold duration were extracted using an algorithm developed by Thompson (2013). Threshold parameters representing the low point of the hydrograph were defined based upon a field-observed discharge that was found to mobilize the D_{50} particle in one of the prototype streams during a multi-year bedload transport sampling campaign (Plumb et al., 2017). The average of each aforementioned event parameter was used to construct characteristic triangular hydrographs, representing average hydrograph characteristics for each land-use scenario (Figure 2). Thus the impacts of progressive

Table II. Land-use scenario descriptions and data sources

Hydrology scenario	Percent urban land use	Study reach	Environment Canada gauge ID	Period
Pre-development (LU1)	<10%	Etobicoke	02HC017	1969–1985
Urbanized (LU2)	40–60%	Mimico	02HC033	1969–1985
Highly urbanized (LU3)	>60%	Mimico	02HC033	1986–2012

hydromodification can be evaluated systematically across different experiments. The duration of each time period was chosen to obtain the largest possible dataset while minimizing the amount of land-use change within each scenario, but it is recognized that there is still some transient land-use change within each scenario. It is acknowledged that another fundamental change with urbanization is the increase in flood peaks (Hollis, 1975). However, the objective here is to address changes associated with hydrograph durations and frequencies, while holding peak discharge constant for each experiment.

The number of hydrographs chosen for each experiment represented 10 years of time in the prototype condition (with time scaled to Mimico Creek by means of Froude similarity). This duration was chosen as a trade-off between ensuring a representative timescale to observe changes in bed morphology and sediment transport characteristics, and the overall length of each experiment. Timescales of quasi-stable bed adjustments in gravel-bed channels are highly variable and are dependent upon a number of factors, including type of disturbance, magnitude of disturbance, timescale of the disturbance and the resilience of the channel. In terms of spatial scales of quasi-stable adjustment, local grain-scale adjustments and micro-scale bedforms tend to occur on the smallest timescales, followed by macro-scale bedforms (such as riffles, bars and pools), changes to the channel cross-section and finally changes to the channel planform and gradient (Knighton, 1998; Buffington, 2012). Knighton (1998) provides an estimated range for the adjustment period of gravel-bed streams ranging between 5 and 100 years. The focuses of these experiments are on changes in bedload transport characteristics (rates, textures and hysteresis) and changes in bed texture (grain-scale changes), and not on macro-scale morphology. The chosen timescale, considered as sufficient, was within the lower end of this range and corresponded to 10 years in prototype condition. The experiments were designed as one-dimensional (no channel meandering) and as such, no bars or 'large-scale' bedforms were expected. Due to the nonlinearity of hydrologic trends between the scenarios and the truncation and removal of low-flow periods between hydrographs, the experiments had different total amounts of water volume and sediment input (Table I), but still represent 10 years of floods with equal peak magnitudes.

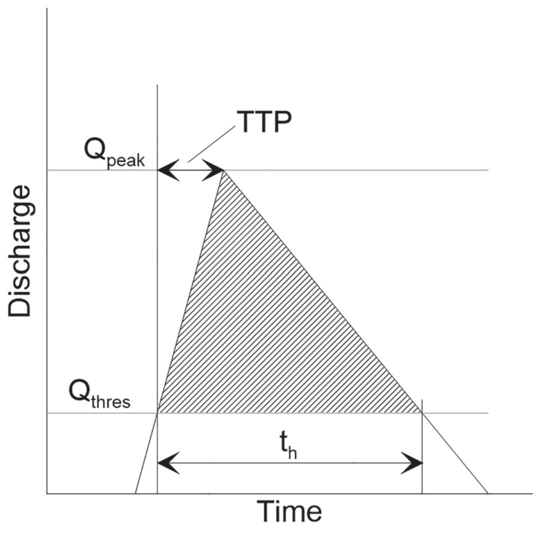

Figure 2. Schematic of parameters extracted from field hydrometric data for the development of laboratory hydrographs corresponding to the land-use scenarios. Q_{peak} and Q_{thres} are peak discharge and threshold discharge, respectively. TTP is time-to-peak and t_h is the threshold duration. See Plumb et al. (2017) for more details.

2.4. Experimental procedure

A pilot test was conducted with the objective of determining the equilibrium slope of the channel. The initial slope was set at 0.005 m/m and the LU1 hydrograph (and corresponding sediment feed) was continuously cycled until an equilibrium slope of 0.01 m/m was achieved after six hydrographs, or approximately 10 h of testing. We recognize that adjusting the slope impacts the Froude similitude between the model and prototype. However, the objective of this study is not to replicate the exact conditions in the prototype condition, but to investigate the impacts of flow regime and unsteady flow on sediment transport dynamics in general. The field data simply motivate the study and provide a general framework of relative changes to the flow regime.

Each experiment began with identical initial conditions. The sediment mixture was placed in the channel and screeded to the initial 0.01 m/m slope. The bed was then slowly saturated and drained to promote initial settlement of the freshly placed sediment. A period of low flow, enough to mobilize sand fractions, with no sediment feed was then initialized to provide the channel with a flow history (Waters and Curran, 2015; Mao, 2018; Redolfi et al., 2018). This period lasted for approximately 8 h, and was considered complete when the sand particles had rearranged such that their mobility was limited in the channel (through visual observation) and there was negligible sediment appearing in the bedload trap. Flow was then stopped and the bed slowly drained for initial bed photos. After the photo inventory, the tailgate was raised, and the channel filled with water to a depth of approximately 0.3 m for the mini echo sounder to be submerged throughout the measurement reach.

Once echo soundings were completed, the bed was slowly drained by lowering the tailgate and a low-flow condition initialized. Flow was subsequently increased monotonically to the first step in the hydrograph (12 L s^{-1} m^{-1}), thereupon the downstream bedload trap was opened and the hydrograph was simulated. After the current hydrograph was completed, flow was quickly reduced (within 5–10 s) to arrest sediment transport and the tailgate slowly raised for the post-hydrograph scan using the echo-sounder. Upon completion of the scan, the channel was slowly drained and post-hydrograph photos acquired of the bed. This process was then repeated for the remaining hydrographs in the experiment. It should be noted that the raising and lowering of the tailgate, draining of the channel and the reinitialization of hydrographs did not cause any significant impact to the bed between experiments (visually verified), with the impacts limited to a few instances of particles rolling or shifting.

2.5. Topographic variability analysis

For each scan, the 20 longitudinal profiles were merged together to create a digital elevation model (DEM), representing the bed topography after each hydrograph. Successive DEMs were compared using DEM differencing and the net volume of both erosion (V_e) and deposition (V_d) were determined. Normalized erosion ($\Delta_{z,e}$) depth was calculated as:

$$\Delta_{z,e} = \frac{V_e}{A_e} \# \quad (2)$$

<NI>where A_e is the planar area of the bed that experienced erosion. Similar calculations were undertaken for the normalized deposition ($\Delta_{z,d}$) depth, using V_d and A_d. Additionally, A_e and A_d were compared against the total planar area (A_T), which is the full area of the 3.5 m long study reach, to determine the

relative fraction of the bed that experienced erosion and deposition. These analyses allow an additional assessment of when the channel reaches an equilibrium condition between hydrographs.

2.6. Bed variability analysis

To assess the change in surface structure and micro-scale bedforms, a bed variability analysis was conducted. Linear regressions were fitted to each of the 20 longitudinal profile scans per hydrograph (Richards, 1976), and the residual values from the regressions used as a metric of bed variability for each specific longitudinal profile. The metric chosen was the root mean square error (RMSE) for each regression, which represents the square root of the residual variance. The median RMSE ($RMSE_{50}$) for the 20 profiles was calculated from the median of the 20 RMSE values from the linear regressions after each hydrograph. This $RMSE_{50}$ parameter represents the overall variability of the bed after each hydrograph. Correspondingly, the standard deviation of the 20 RMSE (σ_{RMSE}) values for each scan were also computed, thus providing a metric for the intra-bed variability (how different the variability of the 20 different profiles is relative to each other) from each scan. All linear regressions for this analysis were found to be statistically significant at the 95% confidence level, with correspondingly high R^2 values ($R^2 \geq 0.95$). Second-order polynomials were also tested, and yielded similar results to the linear models; as such, the linear models were used (Chayes, 1970).

3. Results

3.1. General observations

In each experiment, sediment transport rates and corresponding yields for the first hydrograph were much higher than remaining hydrographs (Figure 3). This has been observed in other sediment-feed laboratory studies (Ferrer-Boix and Hassan, 2014) and is interpreted to be influenced by the initial bed configuration, such that the bed contained a higher content of fine material and had not developed sufficient resistance to the imposed flow conditions, both of which can cause increased bedload transport (Papanicolaou and Schuyler, 2003; Curran and Wilcock, 2005). As such, the first hydrograph eroded a significant amount of material from the bed. This was followed by a period of lower transport (and yields), where the sediment lost in the first hydrograph flush was replenished and the bed gained some structure to resist the flow regime. During this period, very small transport rates were observed during the lower discharges in both the rising and falling limbs, and any considerable transport occurred near the peak. After this period, the sediment transport rates gradually increased and approached a state where, over a cycle of hydrographs,

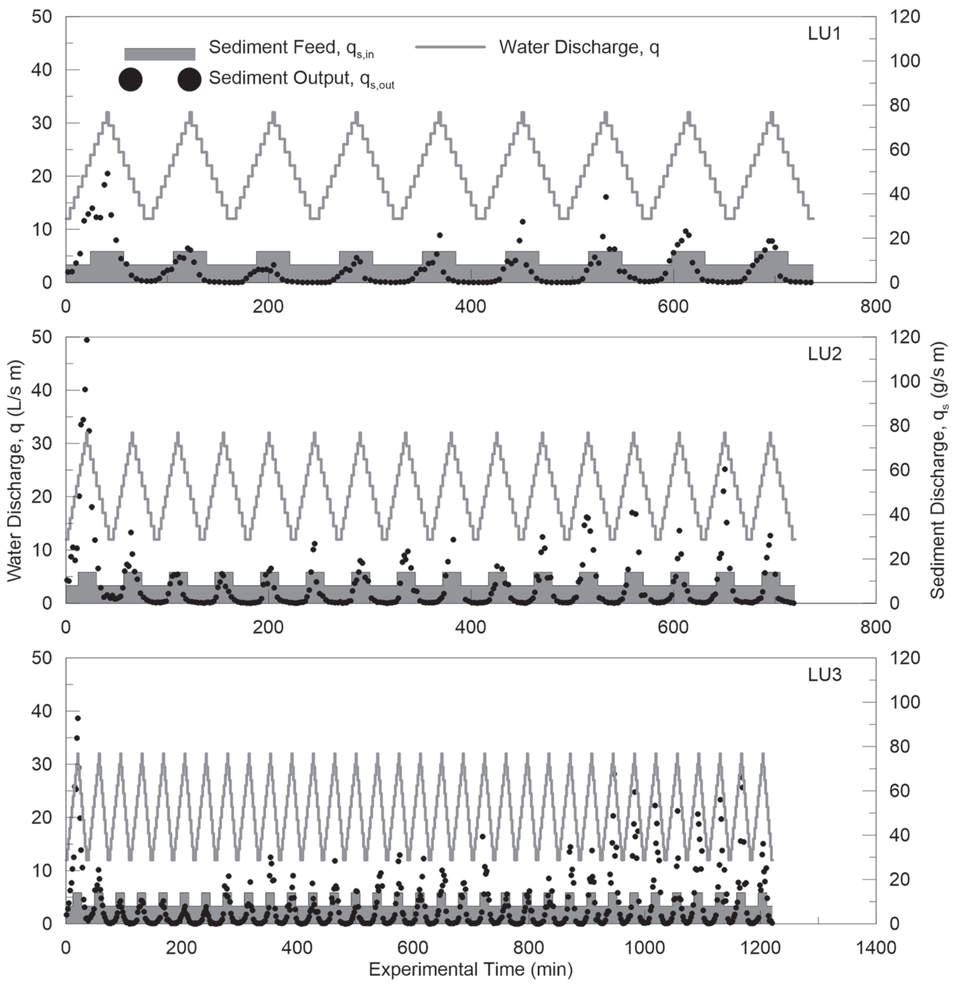

Figure 3. Schematic of laboratory experiments illustrating the experimental stepped hydrographs (grey line), stepped sediment feed rates (grey patches) and bedload transport rates collected from the bedload trap (black dots). Nine, 16 and 33 hydrographs were conducted for LU1, LU2 and LU3, respectively.

the sediment input equaled the sediment output (on a hydrograph basis).

3.2. Topographic variability and slope

Normalized experiment time (see 'Topographic variability analysis', above) versus erosion and deposition for experiments LU1, LU2 and LU3 are illustrated in Figures 4a, 4c and 4e, respectively; where maximum scour depths of 5.0 mm, 8.0 mm and 3.0 mm, respectively, were observed (all corresponding to the initial hydrograph of each experiment).

Consistent with the high yields and transport rates observed after the first hydrograph of each experiment, nearly 100% of the bed in the 3.5 m long study reach exhibited erosion during this period. In subsequent events, deposition trends dominated, which were eventually replaced by alternating erosion and deposition trends in later hydrographs (indicating an approximate balance between erosion and depositional areas). Normalized erosion and deposition depths trended towards a value of approximately 2.0 mm, which is equivalent to D_{50bulk}. More fluctuations occurred in LU3 and LU2, allowing the bed to equilibrate sooner than LU1. LU1 does not reach an equilibrium condition, but it is clearly trending in that particular direction (Figure 4a).

All three experiments have similar average $RMSE_{50}$ values (see 'Bed variability analysis', above) throughout the entire experiment, with $RMSE_{50}$ values of 0.222, 0.213 and 0.218 for LU1, LU2 and LU3, respectively. Variability in $RMSE_{50}$ increased with each experiment (increasing hydrograph frequency), with $RMSE_{50}$ standard deviations of 0.014, 0.017 and 0.022 for LU1, LU2 and LU3, respectively.

Figures 4b, 4d and 4f illustrate the $RMSE_{50}$ values for each scan, as well as the σ_{RMSE} of the 20 RMSE values for each hydrograph (shown by the error bars as $\pm\sigma_{RMSE}$). The increased variability of $RMSE_{50}$ values is visible in LU3. Correspondingly, increases in σ_{RMSE} for LU3 (Figure 4f) – indicating greater topographic variability (higher σ_{RMSE}) – are also visible, which also increases with each subsequent hydrograph (higher standard deviation of $RMSE_{50}$ values). Increased topographic variability with increasing hydrograph frequency and decreasing duration is further accentuated in Figures 4b, 4d and 4f, denoted by the vertical limits of the shaded regions.

Slopes measured from the two profiles in the center of the channel were averaged to estimate the slope after each hydrograph (Figure 5). In all experiments, a reduction in slope occurs after the first hydrograph. This is followed by a gradual increase back to the initial conditions slope. LU1 and LU2 fluctuate around the initial conditions slope of 0.01 m/m for the remainder of the experiment. LU3 fluctuates around the initial conditions slope until approximately half way through the experiment, when the slope slightly increases and fluctuates between 0.01 and 0.012 m/m. LU3 shows the largest range of slopes throughout the experiment as well as the largest relative slope adjustment between consecutive hydrographs.

3.3. Bedload transport rates and yields

For the LU1 experiment, overall transport rates were lower than those of LU2 and LU3. This included both initial higher rates observed in the first hydrograph and subsequent rates as the experiments progressed. Transport rates corresponding to the peak discharge of each hydrograph are shown in Figure 6. Normalized time for each hydrograph is the ratio between the

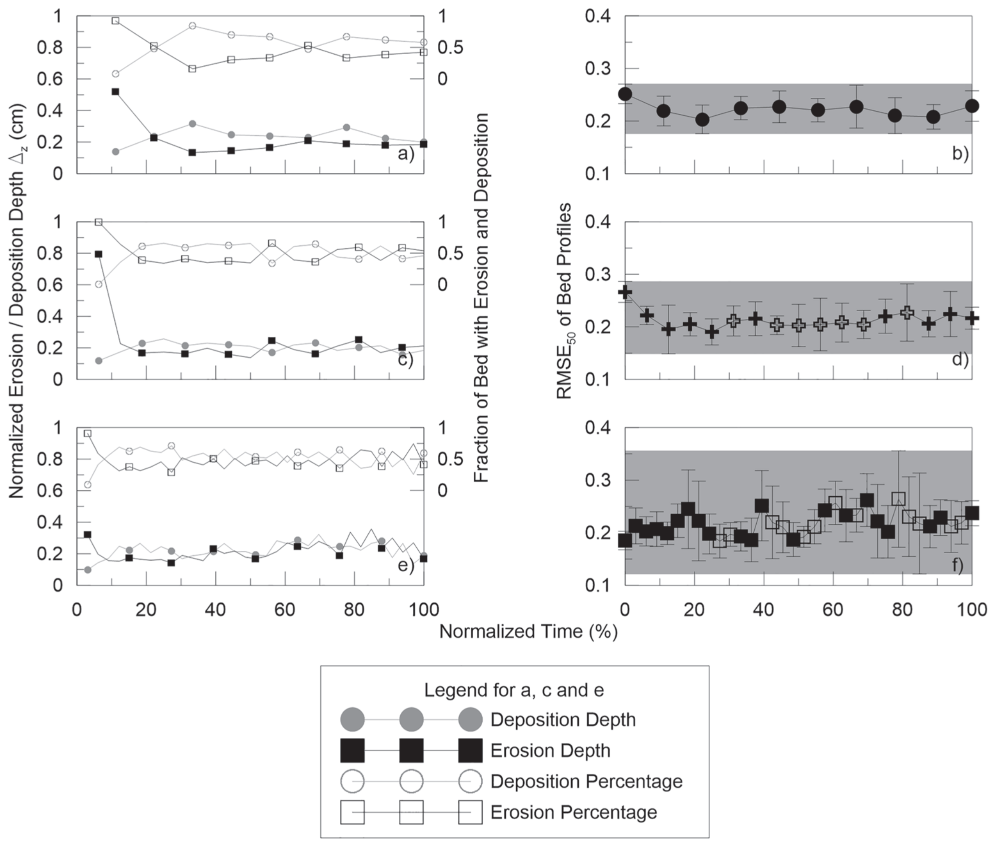

Figure 4. Normalized erosion and deposition depths and the proportion of the bed undergoing erosion and deposition for (a) LU1, (c) LU2 and (e) LU3. Median RMSE of the 20 profiles in ($RMSE_{50}$) each bed scan, where the error bars represent one standard deviation of the RMSE values (σ_{RMSE}). See text for details. Solid and hollow symbols in (b), (d) and (f) represent hydrographs exhibiting clockwise hysteresis and counterclockwise hysteresis, respectively. Grey patches depict the range of bed variability for each experiment.

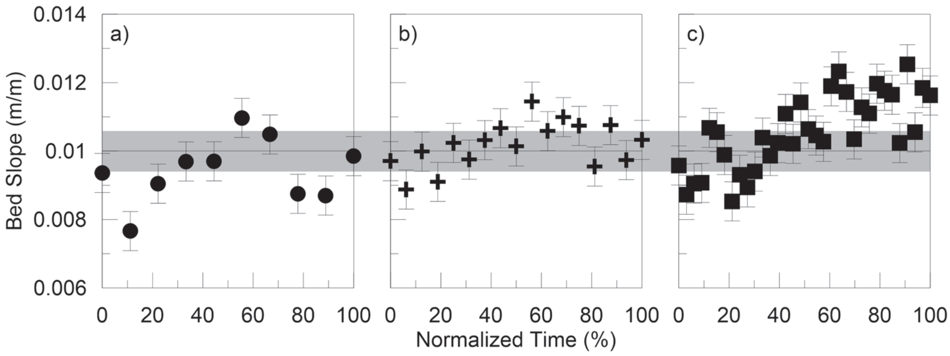

Figure 5. Slope adjustments throughout (a) LU1, (b) LU2 and (c) LU3. Error bars represent measurement error associated with mini echo-sounder. Shaded box represents possible error associated with initial conditions slope.

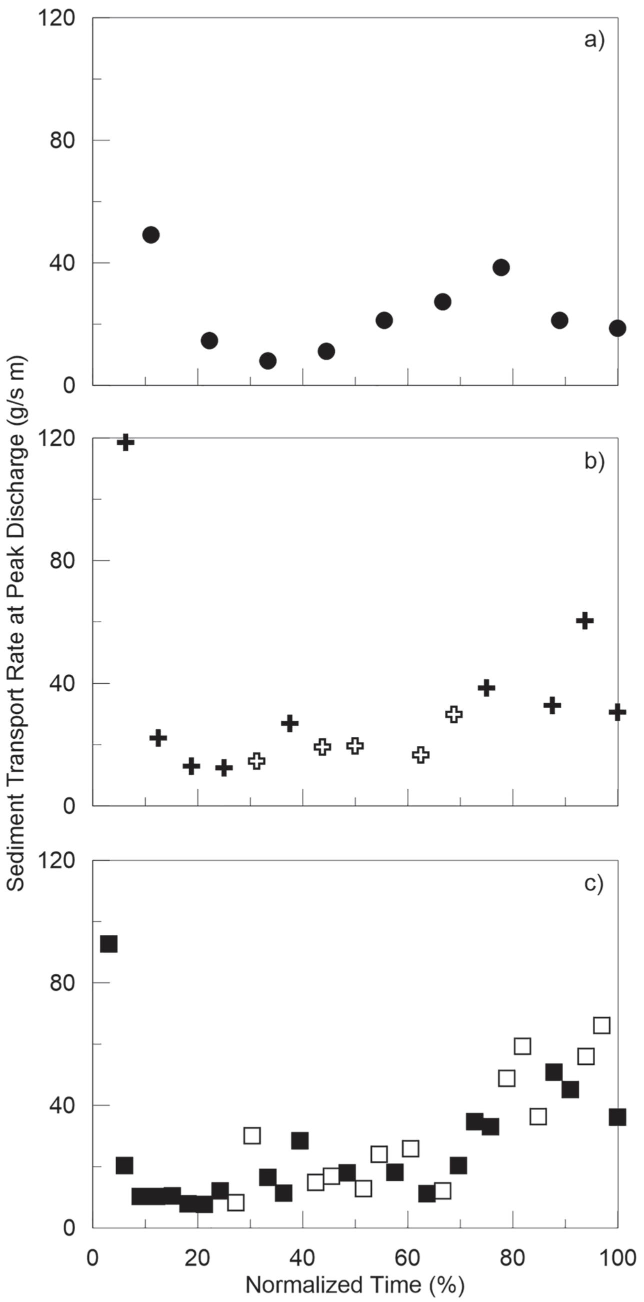

Figure 6. Sediment transport rates corresponding to the peak discharge of each hydrograph. Solid and hollow symbols represent hydrographs exhibiting clockwise hysteresis and counterclockwise hysteresis, respectively. Note: no counterclockwise hysteresis was observed in LU1.

number of that specific hydrograph and the total number of hydrographs in the experiment (expressed as a percentage). Excluding the first hydrograph in each experiment, the maximum transport rate for LU1 at peak discharge was approximately $40\,g\,s^{-1}\,m^{-1}$, whereas LU2 and LU3 both have transport rates above $60\,g\,s^{-1}\,m^{-1}$. LU2 and LU3 exhibit similar trends; they both have longer periods of low sediment transport rates, followed by an increase until the rates appear to stabilize, although with considerable variability inherent in bedload transport. This final period of relatively stable transport rates is more pronounced in LU3, as the rates appear to stabilize at approximately $50\,g\,s^{-1}\,m^{-1}$, with the variability being $\pm 14\,g\,s^{-1}\,m^{-1}$ (Figure 6c).

Notable bedload hysteresis was observed during the hydrographs. A selection from each experiment is presented in Figure 7, with hydrographs chosen near the beginning, middle and end of each experiment to illustrate the evolution of bedload hysteresis throughout experiment. For example, LU1-H5 refers to the fifth hydrograph in the LU1 experiment. Clockwise hysteresis or a combination of single value plus clockwise loop was observed for all hydrographs in LU1 (Figure 7, top row). For LU2 (Figure 7, middle row) and LU3 (Figure 7, bottom row), the hysteresis was much more varied, with all five of the common classes being exhibited as the experiments progressed. However, in general, the hysteresis loops were much tighter for these shorter hydrographs, resembling more a single-value hysteresis with occasional small loops. The higher transport rates of LU2 and LU3 relative to LU1 are further illustrated in Figure 7.

In all experiments, the output yield (Y_{out}), which is the total mass of sediment collected in the bedload trap for each hydrograph, was much higher for the initial hydrograph than the input yield (Y_{in}), which is the total mass of sediment input during each hydrograph. Subsequent hydrographs in each experiment observed lower yields, averaging outputs between 25% and 30% of their respective inputs, and slowly increasing until the output approximately equaled the input, which also corresponded to the stabilization of the transport rates previously noted (Figure 6). LU1 never achieved a quasi-steady state in transport, with a maximum Y_{out}/Y_{in} ratio of approximately 0.6 (Figure 8a). Both LU2 and LU3 progressed to a $Y_{out}/Y_{in} \approx 1.0$ after 12 and 25 hydrographs, respectively, and oscillated about this condition for the duration of each experiment (Figures 8b and 8c). A major difference between LU1 and either LU2 or LU3 was the yield derived from the rising and falling limbs of the hydrographs. Figures 8d, 8e and 8f illustrate the ratio of the rising limb output yield (Y_r) to the falling limb output yield (Y_f), herein referred to as the hysteresis ratio (H_r). $H_r = 1.0$ indicates that yields are balanced between the rising and falling limbs of the hydrograph, whereas $H_r > 1.0$ and $H_r < 1.0$ correspond to clockwise and counterclockwise hysteresis,

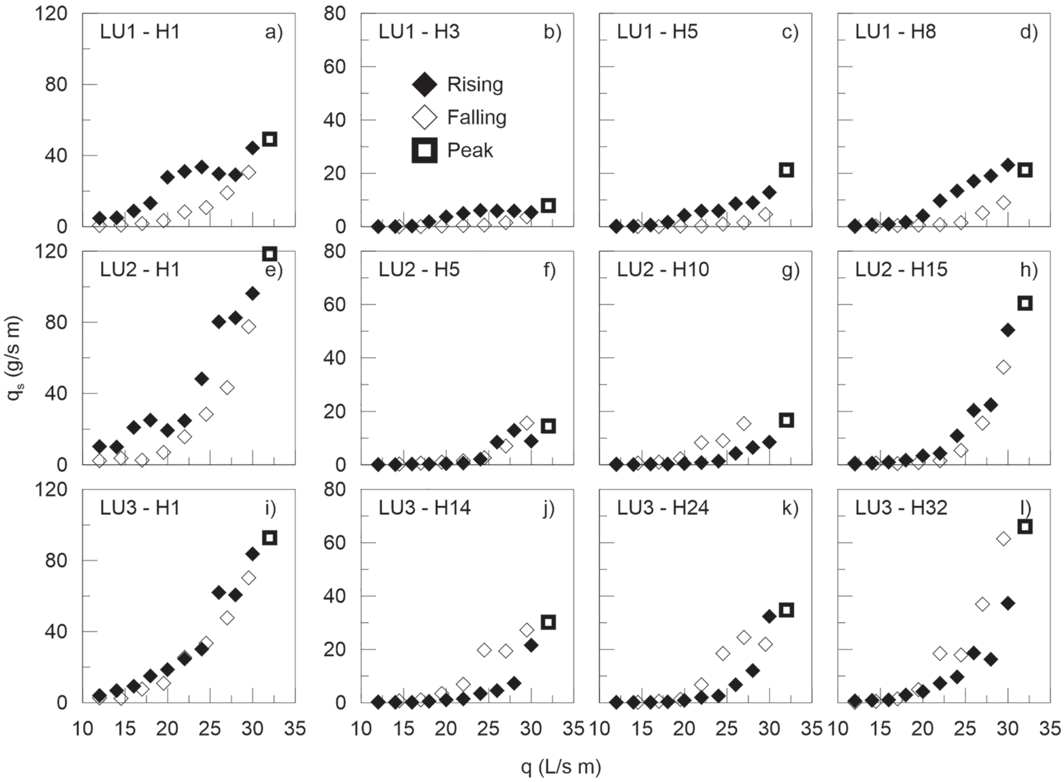

Figure 7. Phase plots for selected hydrographs from each experiment (LU1 top row, LU2 middle row, LU3 bottom row) illustrating the different phases of bedload hysteresis present. H_i denotes the hydrograph number of that specific experiment.

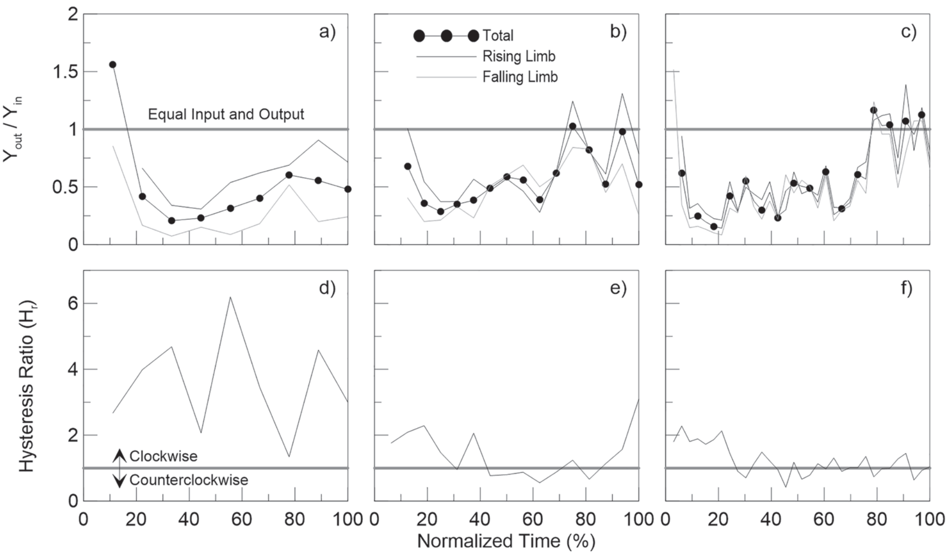

Figure 8. Sediment yield ratios (Y_{out}/Y_{in}) of each hydrograph for the total yield, rising limb yield and falling limb yield for (a) LU1, (b) LU2 and (c) LU3 and the hysteresis ratio (H_r) (ratio of the rising limb yield and falling limb yield) for (d) LU1, (e) LU2 and (f) LU3. The horizontal line serves as a threshold for equal input and output sediment yields (top) and clockwise or counterclockwise nature of the hysteresis loops (bottom).

respectively. For all experiments, $H_r > 1.0$ for the first few hydrographs of each test. For LU2 and LU3, $H_r \rightarrow 1.0$ after seven and nine hydrographs, respectively, and subsequently oscillated about $H_r \cong 1.0$ (ranging between $0.6 \leq H_r \leq 1.4$). The observed exception is in the final two hydrographs of LU2, which shows a strong clockwise hysteresis. The average H_r for each experiment was 3.6, 1.4 and 1.2 for LU1, LU2 and LU3, respectively. Greater variability is also observed with the hysteresis of experiment LU1, with a range in H_r of 4.9, compared to ranges of 2.5 and 1.9 for LU2 and LU3, respectively.

3.4. Bedload size

The D_{30load}, D_{50load} and D_{90load} percentiles were chosen to characterize the lower, median and larger particle sizes of the bedload transported through the channel, respectively. Figure 9 illustrates particle percentiles for bedload samples corresponding to Q_{peak}. Similar trends for all experiments are observed for the coarsest particles in the bedload (D_{90load}), where D_{90load} for the first few hydrographs (only the first in the case of LU1) are finer than the D_{90bulk} of 7.0 mm (Figures 9a,

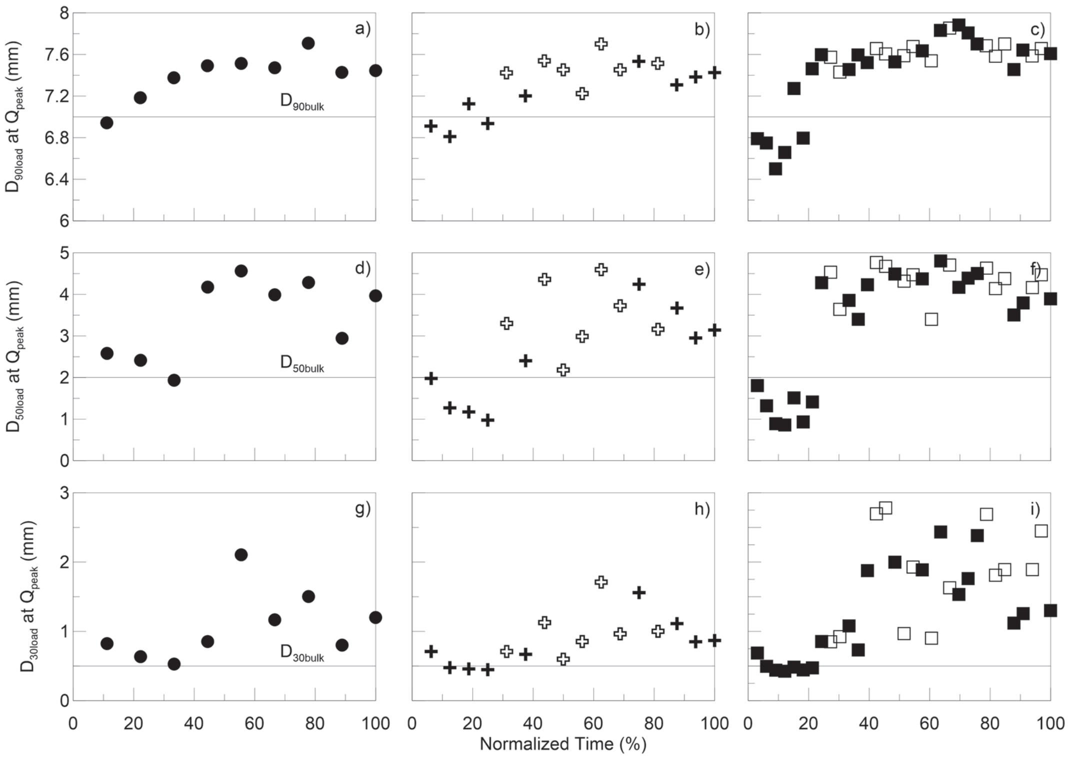

Figure 9. 90th percentile of the bedload transported out of the channel (D_{90load}) at peak discharge for each hydrograph for (a) LU1, (b) LU2 and (c) LU3. 50th percentile of the bedload (D_{50load}) at peak discharge for each hydrograph for (d) LU1, (e) LU2 and (f) LU3. 30th percentile of the bedload (D_{30load}) at peak discharge for each hydrograph for (g) LU1, (h) LU2 and (i) LU3. Solid and hollow symbols represent hydrographs exhibiting clockwise hysteresis and counterclockwise hysteresis, respectively. Note: no counterclockwise hysteresis was exhibited in LU1.

9b and 9c). Grain sizes gradually increase to values coarser than the D_{90bulk} and stabilize at values of approximately 7.5 mm.

D_{50load} for LU1 begins slightly coarser than the D_{50bulk} of 2.0 mm but coarsens abruptly to approximately 4.0 mm after the third hydrograph (Figure 9d). A similar trend is observed for LU2, with the exception that a brief period of fining of D_{50load} occurs after the first hydrograph, with a less abrupt increase (Figure 9e). Also, there is a noted gradual fining of the final six hydrographs in LU2, with $D_{50load} \rightarrow D_{50bulk}$. D_{50load} of LU3 similarly begins finer than the D_{50bulk}, which abruptly increases, similar to the other experiments, here averaging 4.0 mm (Figure 9f). There is less of a downward trend noted in grain size of LU3 as the experiment progresses (relative to the other experiments), indicating that the median size remained relatively constant at peak discharge for LU3.

LU1 and LU2 exhibit similar trends in D_{30load}. The experiments begin with $D_{30load} \approx D_{30bulk} \approx 0.5$ mm, which gradually increase to $D_{30load} \approx 1.5$ mm (with the exception of hydrograph 5 in LU1) and then trend back towards the D_{30bulk} (Figures 9g and 9h). LU3 exhibits a much different trend (Figure 9i); the first several hydrographs remain similar to D_{30bulk}; however, the mean and variance notably increase as the experiment progresses, with the latter hydrographs possessing a range between 1.0 mm and 2.8 mm. This change occurs when bedload hysteresis patterns begin to fluctuate between clockwise and counterclockwise modes of transport.

Bedload percentiles also exhibit hysteresis effects with the rising and falling limb of each hydrograph. In general, bedload was observed to be coarser on the rising limbs (Figure 10). Figure 10 illustrates ratio between D_{30load}, D_{50load} and D_{90load} obtained on the rising limb versus the falling limb, similar to the H_r metric previously introduced. In all experiments, D_{90load} exhibited little hysteresis, remaining similar on both the rising and falling limbs. D_{30load} exhibited a range between clockwise and counterclockwise hysteresis and was similar for all experiments. D_{50load} had less hysteresis for LU3 relative to the other two experiments.

Hysteresis trends in all experiments for D_{90load} exhibit similar trends, exhibiting a gradual coarsening as each experiment progressed, with mostly single-value hysteresis trends ($H_r \approx 1.0$) or having slight clockwise trends. Hysteresis patterns of D_{50load} are more variable than the previously noted grain sizes and tend to steepen as each experiment progressed, indicating a more abrupt change in D_{50load} with increasing or decreasing discharge. Hysteresis trends of D_{30load} remain similar for LU1 (Figure 7), become slightly steeper for LU2 (Figure 7) and notably steeper and coarser for LU3 (Figure 7), further enforcing the higher variability observed in Figure 9i. Samples obtained that were smaller than approximately 200 g were not sieved and are not included in these figures, as meaningful grain-size analysis on such a small sample size could not be reliably obtained.

3.5. Bed surface texture

In all experiments, armor layers developed on the channel bed, with their surface percentiles D_{90surf}, D_{50surf} and D_{30surf} all coarser than their respective bulk mixture parameters (Figure 11). The experiments all begin with a slightly coarser bed than their bulk mixtures, which is attributed to the period of water working to establish flow histories. D_{90surf} for all experiments shows more scatter than the smaller percentiles. LU2 and LU3 both have similar average surface textures throughout the experiments, with average $D_{90surf} \approx 8.5$ mm, $D_{50surf} \approx 4.5$ mm and $D_{30surf} \approx 3.5$ mm. LU1 coarsens to a greater extent until approximately midway through the experiment, when it exhibits a period of fining and approaches the equilibrium values of LU2 and LU3, although still slightly coarser. For LU2 and LU3, the most abrupt changes in surface texture correspond to hydrographs that exhibited a counterclockwise bedload hysteresis.

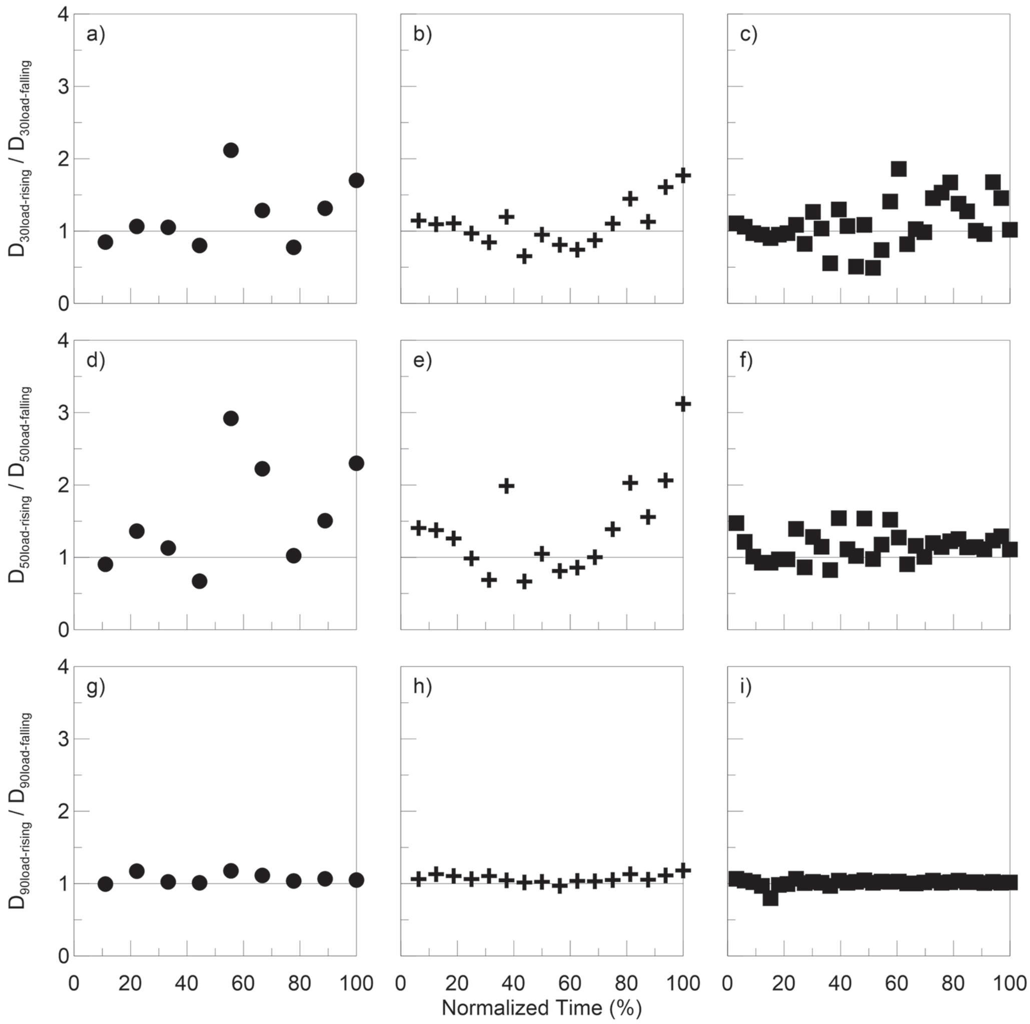

Figure 10. Ratio of $D_{30\text{load}}$ on the rising and falling limbs for (a) LU1, (b) LU2 and (c) LU3. Ratio of $D_{50\text{load}}$ on the rising and falling limbs for (d) LU1, (e) LU2 and (f) LU3. Ratio of $D_{90\text{load}}$ on the rising and falling limbs for (g) LU1, (h) LU2 and (i) LU3.

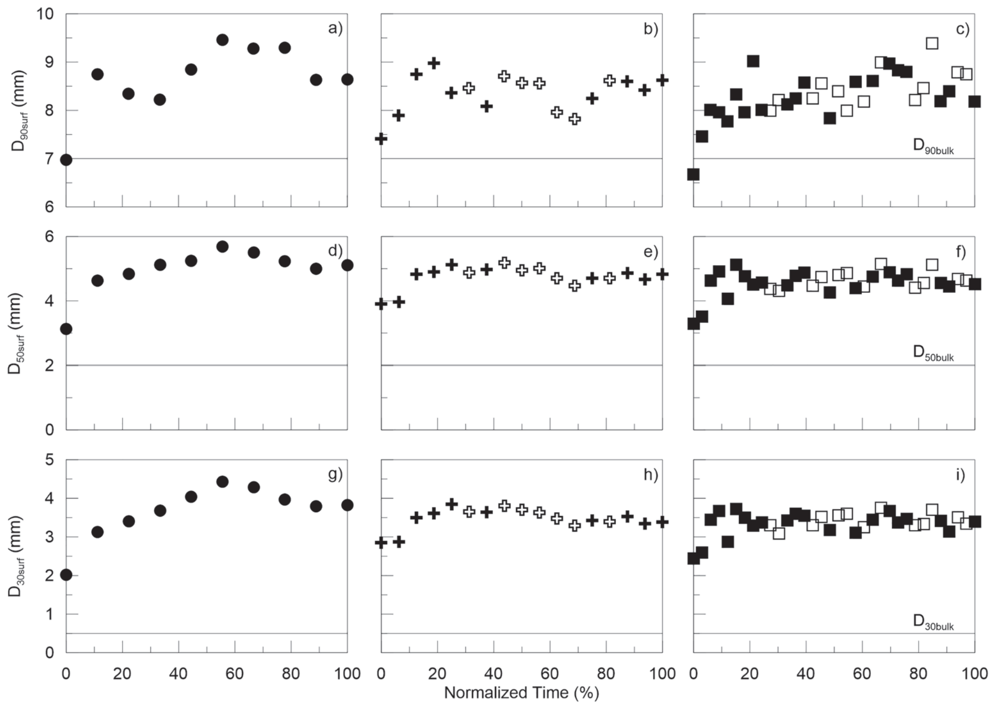

Figure 11. 90th percentile of the surface ($D_{90\text{surf}}$) after each hydrograph for (a) LU1, (b) LU2 and (c) LU3. 50th percentile of the surface ($D_{50\text{surf}}$) after each hydrograph for (d) LU1, (e) LU2 and (f) LU3. 30th percentile of the surface ($D_{30\text{surf}}$) at peak discharge for each hydrograph for (g) LU1, (h) LU2 and (i) LU3. Solid and hollow symbols represent hydrographs exhibiting clockwise hysteresis and counterclockwise hysteresis, respectively.

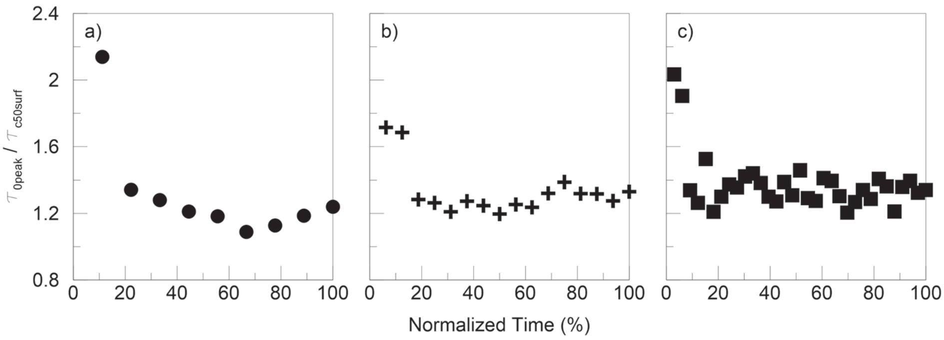

Figure 12. Ratio of applied shear stress at Q_{peak} (τ_{peak}) to critical shear stress ($\tau_{c50surf}$) for D_{50surf} for (a) LU1, (b) LU2 and (c) LU3.

The ratio between the applied shear stress at peak discharge (τ_{0peak}) and the critical shear stress for D_{50surf} ($\tau_{c50surf}$) was examined for each experiment (Figure 12). In all experiments, the first hydrograph greatly exceeded the shear stress of the D_{50surf}. As the bed coarsened throughout the experiments, the ratio reduced to between approximately 1.2 and 1.4, and remained relatively stationary. LU1, which was found to have a coarser bed, had a correspondingly lower ratio, ranging between 1 and 1.4. D_{50load} and D_{50surf} was compared to the fraction of time each hydrograph exceeded $\tau_{c50surf}$ (Figure 13). The first hydrograph in LU1 and the first two hydrographs in LU2 and LU3 entirely exceed the $\tau_{c50surf}$. A lower fraction of time exceeds $\tau_{c50surf}$ for the remaining hydrographs in LU1 relative to the two other experiments. Correspondingly, a higher fraction of time exceeds $\tau_{c50surf}$ for LU3 relative to the other two experiments. With increasing unsteadiness, the D_{50load} gets larger and nearly approximates the D_{50surf} (Figure 11c). The relative change in D_{50surf} was also compared to the fraction of time exceeding $\tau_{c50surf}$ for each hydrograph. Aside from the first hydrograph, which significantly coarsened the bed, the most unsteady experiment (LU3) had the most impact on bed texture between successive hydrographs. This is especially true for fining, where up to a 20% reduction in D_{50surf} was observed.

4. Discussion

4.1. Hydrograph shape on bedload transport hysteresis and changes in bed texture

Longer duration hydrographs (LU1) exhibited hysteresis ratios greater than 1, with significantly less material being transported on the falling limbs. Shorter duration hydrographs exhibited hysteresis ratios close to 1.0, which oscillated about unity, in either clockwise or counterclockwise trends. As mentioned above, this oscillation also corresponded to a departure from bulk values of the bedload percentiles (Figures 9e, 9f, 9h and 9i) and a steepening of the bedload size hysteresis (Figure 7).

Figure 14 illustrates the normalized relative sediment yields, which is the sediment output normalized by the total work index (Y_{out}/W_k) for (a) all hydrographs (combination of both rising and falling limbs), (b) the rising limbs of all hydrographs and (c) the falling limbs of all hydrographs for each experiment. The yield from the first hydrograph of each experiment was not included, owing to the much higher rates (previously discussed). Figure 14 further illustrates that, independently of sediment input, shorter duration hydrographs transport a proportionately larger load, which primarily results from the yield on the falling limb. Observations on falling limb duration had been hypothesized by Hassan et al. (2006) to be a critical factor governing the amount of vertical sorting of the bed, with shorter durations resulting in insufficient time for the sorting process to occur. Hassan et al. (2006) also attributed observed clockwise hysteresis to the sediment-starved nature of the experimental channel, as their experiments were conducted with no sediment supply. In this study, experiments had identical sediment supply rates, with only the duration of sediment supply varied (derived from the differing hydrograph durations); however, the development of an armor layer in these experiments suggests that these experiments are also supply limited. The slightly coarser bed texture corresponding to the longer duration hydrographs (Figure 11) supports the possibility of vertical sorting being a contributing factor for the observed differences in transport rates.

Bedload hysteresis trends appear to influence the variability in bedload percentiles, as the bedload percentiles in LU2 and LU3 begin to depart from the bulk values when the hysteresis trends begin to switch between clockwise and counterclockwise (Figures 9e, 9f, 9h and 9i), approaching an H_r of 1. Bedload hysteresis direction was also linked to relative changes in bed surface texture. Clockwise bedload hysteresis corresponded to 66%, 75% and 54% of the instances of bed coarsening for LU1, LU2 and LU3, respectively (Figure 13). Shorter duration hydrographs transport a larger proportional

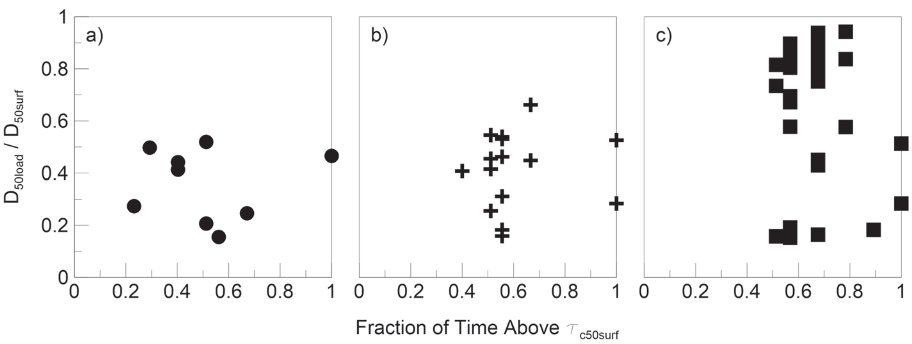

Figure 13. Ratio of D_{50load} to D_{50surf} as a function of the fraction above critical shear stress ($\tau_{c50surf}$) for D_{50surf} for each hydrograph in (a) LU1, (b) LU2 and (c) LU3.

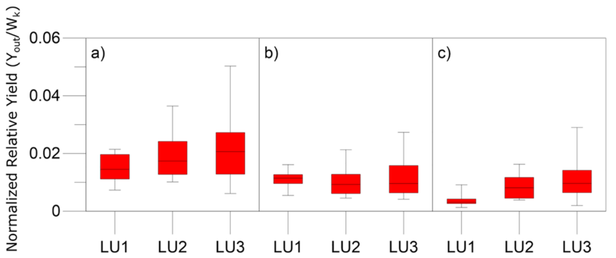

Figure 14. Normalized relative yield (Y_{out}/W_k) for (a) total yield (combination of rising and falling limbs), (b) rising limb yield and (c) falling limb yield for all hydrographs in each experiment, excluding the first hydrograph. [Colour figure can be viewed at wileyonlinelibrary.com]

load on the falling limb and, correspondingly, the bed has less time to develop an armor layer through vertical sorting. Conversely, the longer duration hydrographs transport a proportionally smaller load during the falling limb due to more time for vertical sorting, particle rearrangements and surface restructuring, resulting in the development of an armor layer and an increase in critical shear stress (Hassan et al., 2006; Mao, 2012). The lower prediction for LU3 is speculated to be influenced by the increased topographic variability of the bed, which is confounding the lag between discharge, transport and the resulting bed texture. Neither topographic variability nor surface texture was measured throughout the hydrographs; thus specific results related to fining and coarsening during specific hydrograph limbs (e.g. Hassan et al., 2006; Mao, 2012; Wang et al., 2015) cannot be inferred.

4.2. Hydrograph shape and magnitude of channel adjustment

The shorter duration hydrographs result in larger relative magnitudes of channel adjustment than the corresponding longer duration hydrographs. There are greater adjustments to overall topographic variability (Figure 4), slope (Figure 5) and bed surface texture (Figure 14). The relatively larger adjustments are hypothesized to result from the channel having insufficient time to adjust to the changing flow conditions (Plate, 1994), which results in a proportionately larger exceedance of critical shear. The shear exceedance leads to higher bedload transport rates (Figure 6), larger sediment yields (Figures 8 and 14) and a coarser transported load (Figures 9 and 13), all of which contribute to the larger adjustments observed in the shorter duration hydrograph experiments.

Shorter duration hydrographs resulted in larger changes in bed variability after successive hydrographs and greater intrabed variability between the hydrographs. Although the exact reason for this increased bed variability remains unknown, there are a number of possible contributing factors. The shorter falling hydrograph limbs of experiment LU3 may allow less time for the bed to reorganize after the peak, which is also supported by the higher transport rates observed on the falling limbs, relative to LU1. Although not physically quantified, a number of microform clusters were observed to develop on the bed, and the increased variability could be clusters forming as an additional energy dissipation mechanism (Papanicolaou and Schuyler, 2003; Tan and Curran, 2012) to account for the flashy, frequent events in LU3. This more variable bed structure is hypothesized to be diminishing the entrainment rate of the sand grains by sheltering them from the flow, which is supported by the increased variability of D_{30load} for LU3 (Figure 9i) and the slightly finer bed texture of LU3 relative to LU1 (Figure 11).

5. Conclusions

Laboratory experiments were conducted to investigate how unsteady flows and changes in the flow regime impact bedload transport rates and channel morphology in a gravel-bed channel. The experiments are motivated from a larger study on the impacts of urbanization on sediment dynamics in gravel-bed rivers, inspired from field data and observations, but assessing the channel responses in order for the results to be generalized to basic changes in flow regime and hydrograph shape. Three hydrologic conditions (experiments) representing different levels of basin urbanization (flow regimes) were derived from hydrometric gauge data of urbanizing watersheds in Ontario, Canada. Each experiment consisted of a series of hydrographs with equal peak discharge and varying duration. A hysteresis ratio metric was introduced to quantify the bedload hysteresis.

Longer duration hydrographs resulted in lower sediment transport rates, clockwise hysteresis loops and less topographic variability in the channel bed. Conversely, shorter duration hydrographs resulted in higher transport rates, more variable hysteresis, but generally closer to single value, and more topographic bed variability. Changes in bedload hysteresis were attributed to vertical sorting and additional sheltering from larger grains, which is supported by the coarser bed of the longer duration hydrographs and topography scans. The direction of bedload hysteresis was also tied to changes in bed texture, with clockwise hysteresis commonly resulting in bed coarsening.

Shorter duration and more frequent hydrographs resulted in larger relative bed adjustments, including topographic variability, slope and bed surface texture. These larger adjustments are hypothesized to result from an insufficient time for the channel to adjust to the changing flow, which results in a larger proportion of the hydrograph exceeding critical thresholds, with bedload having higher rates and coarser sizes. This contradicts previous experiments indicating that more frequent unsteady flow pulses resulted in a decrease in bedload transport. Increased topographic variability associated with the flashiest hydrographs is hypothesized to be a manifestation of these rapid adjustments, which serves to dissipate excess energy. The higher and coarser bedload transport rates, larger proportional yields and larger relative bed adjustments emphasize that increases in flood frequency and flashiness in concert with decreases in flood duration amplify morphologic adjustments.

The outcomes of this research are important given the well-documented ecological and morphological impacts due to changing flow regimes as a result of watershed land-use changes (Walsh et al., 2005; Chin, 2006). With precipitation trends changing at the global scale (Zhang et al., 2007), rivers will continue to become more impacted by changes in flow regime.

Acknowledgements—Special thanks are extended to Prof. Anton J. Schleiss for providing laboratory resources to conduct these experiments. We thank Jesús Sánchez Alcalde for assisting with the experiments. This project was supported by funding from an NSERC IPS (McKie), by the H2020-MSCA-IF-2018 programme (Marie Sklodowska-Curie Actions) of the European Union under REA grant agreement number 834329-SEDILAND (Juez) and by Water Regime Investigations and Simulations Ltd, JTB Environmental Systems Inc. and R&M Construction (Plumb).

Data Availability Statement

Data from these experiments are available from the corresponding author upon request.

Conflict of Interest

The authors have no conflict of interest to declare..
Key Points

- Unsteady flow lab experiments designed from field data to evaluate the impact of urbanization on sediment transport in gravel-bed channels
- Differences in transport rates, textures and hysteresis found for hydrographs of different flashiness and duration
- Flashier hydrographs (more urban land-use) found to result in greater bed topographic variability

References

Annable WK, Watson CC, Thompson PJ. 2012. Quasi-equilibrium conditions of urban gravel-bed stream channels in southern Ontario, Canada. *River Research and Applications* **28**(3): 302–325. https://doi.org/10.1002/rra.1457.

Bakker M, Antoniazza G, Odermatt E, Lane SN. 2019. Morphological response of an alpine braided reach to sediment-laden flow events. *Journal of Geophysical Research* **124**(5): 1310–1328.

Bernhardt E, Palmer M, Allan J.D, Alexander G.J., Barnas K, Brooks SS, Carr J, Clayton S, Dahm C, Follstad S.J, Galat D, Gloss S, Goodwin P, Hart D, Hassett B, Jenkinson R, Katz S, Kondolf G, Sudduth E. 2005. Synthesizing U.S. River Restoration Efforts. *Science (New York, N.Y.)* **308**: 636–7. https://doi.org/10.1126/science.1109769

Bombar G, Elci S, Tayfur G, Guney S, Bor A. 2011. Experimental and numerical investigation of bed-load transport under unsteady flows. *Journal of Hydraulic Engineering* **137**(10): 1276–1282. https://doi.org/10.1061/(asce)hy.1943-7900.0000412.

Booth DB. 1990. Stream-channel incision following drainage-basin urbanization. *Journal of the American Water Resources Association* **26** (3): 407–417. https://doi.org/10.1111/j.1752-1688.1990.tb01380.x.

Buffington JM. 2012. Changes in channel morphology over human time scales. In *Gravel-Bed Rivers: Processes, Tools, Environments*, Church M, Biron PM, Roy AG (eds). Wiley: Chichester, UK; 435–463.

Chayes F. 1970. On deciding whether trend surfaces of progressively higher order are meaningful. *Geological Society of America Bulletin* **81**(4): 1273–1278.

Chin A. 2006. Urban transformation of river landscapes in a global context. *Geomorphology* **79**: 460–487. https://doi.org/10.1016/j.geomorph.2006.06.033.

Curran JC, Wilcock PR. 2005. Effect of sand supply on transport rates in a gravel-bed channel. *Journal of Hydraulic Engineering* **131**(11): 961–967. https://doi.org/10.1061/(ASCE)0733-9429(2005)131:11(961).

Ferrer-Boix C, Hassan MA. 2014. Influence of the sediment supply texture on morphological adjustments in gravel-bed rivers. *Water Resources Research* **50**(11): 8868–8890. https://doi.org/10.1002/2013WR015117.

Ferrer-Boix C, Hassan MA. 2015. Channel adjustments to a succession of water pulses in gravel bed rivers. *Water Resources Research* **51** (11): 8773–8790. https://doi.org/10.1002/2015WR017664.

Gregory KJ. 2006. The human role in changing river channels. *Geomorphology* **79**: 172–191. https://doi.org/10.1016/j.geomorph.2006.06.018.

Guillén-Ludeña S, Franca MJ, Cardoso AH, Schleiss AJ. 2015. Hydromorphodynamic evolution in a 90° movable bed discordant confluence with low discharge ratio. *Earth Surface Processes and Landforms* 1927-1938. https://doi.org/10.1002/esp.3770.

Gunsolus EH, Binns AD. 2017. Effect of morphologic and hydraulic factors on hysteresis of sediment transport rates in alluvial streams. *River Research and Applications* **28**(3): 1–10. https://doi.org/10.1002/rra.3184.

Hassan MA, Church M. 2001. Sensitivity of bed load transport in Harris Creek: seasonal and spatial variation over a cobble-gravel bar. *Water Resources Research* **37**(3): 813–825. https://doi.org/10.1029/2000WR900346.

Hassan MA, Egozi R, Parker G. 2006. Experiments on the effect of hydrograph characteristics on vertical grain sorting in gravel bed rivers. *Water Resources Research* **42**: W09408. https://agupubs.onlinelibrary.wiley.com/action/showCitFormats?doi=10.1029/2005WR004707.

Hollis GE. 1975. The effect of urbanization on floods of different recurrence interval. *Water Resources Research* **11**(3): 431–435. https://doi.org/10.1029/WR011i003p00431.

Humphries R, Venditti JG, Sklar LS, Wooster JK. 2012. Experimental evidence for the effect of hydrographs on sediment pulse dynamics in gravel-bedded rivers. *Water Resources Research* **48**: W01533. https://doi.org/10.1029/2011WR010419.

Juez C, Hassan MA, Franca MJ. 2018. The origin of fine sediment determines the observations of suspended sediment fluxes under unsteady flow conditions. *Water Resources Research* **48**: WR022982. https://doi.org/10.1029/2018WR022982.

Knighton D. 1998. *Fluvial Forms and Processes: A New Perspective*. Oxford University Press: New York.

Kuhnle RA. 1992. Bed load transport during rising and falling stages on two small streams. *Earth Surface Processes and Landforms* **17**(2): 191–197. https://doi.org/10.1002/esp.3290170206.

Lane EW. 1955. The importance of fluvial morphology in hydraulic engineering. *Proceedings of the American Society of Civil Engineers* **81**: 1–17.

Lee KT, Liu Y-L, Cheng K-H. 2004. Experimental investigation of bedload transport processes under unsteady flow conditions. *Hydrological Processes* **18**(13): 2439–2454. https://doi.org/10.1002/hyp.1473.

Lenzi MA, Mao L, Comiti F. 2006. Effective discharge for sediment transport in a mountain river: computational approaches and geomorphic effectiveness. *Journal of Hydrology* **326**(1–4): 257–276. https://doi.org/10.1016/j.jhydrol.2005.10.031.

Leopold LB, Wolman MG, Miller JP. 1964. *Fluvial Processes in Geomorphology*. Dover Publications: New York.

Mao L. 2012. The effects of flood history on sediment transport in gravel-bed rivers. *Journal of Geophysical Research* **117**: 196-205 F03024. https://doi.org/10.1029/2012JF002428.

Mao L. 2018. The effect of hydrographs on bed load transport and bed sediment spatial arrangement. *Geomorphology* **322**: 196–205. https://doi.org/10.1016/j.geomorph.2018.08.046.

Martin RL, Jerolmack DJ. 2013. Origin of hysteresis in bed form response to unsteady flows. *Water Resources Research* **49**(3): 1314–1333. https://doi.org/10.1002/wrcr.20093.

Matos JP, Hassan MA, Lu XX, Franca MJ. 2018. Probabilistic prediction and forecast of daily suspended sediment concentration on the Upper Yangtze River. *Journal of Geophysical Research* **8**: 1982–2003. https://doi.org/10.1029/2017JF004240.

Mrokowska MM, Rowinski PM. 2019. Impact of unsteady flow events on bedload transport: a review of laboratory experiments. *Water* **11** (5): 907. https://doi.org/10.3390/w11050907.

Mrokowska MM, Rowinski PM, Ksiazek L, Struzynski A, Wyrebek M, Radecki-Pawlik A. 2016. Flume experiments on gravel bed load transport in unsteady flow: preliminary results. In *Hydrodynamic and Mass Transport at Freshwater Aquatic Interfaces: 34th International School of Hydraulics*, Rowinski PM, Marion A (eds). Springer: Berlin; 221–233.

Papanicolaou T, Schuyler A. 2003. Cluster evolution and flow-frictional characteristics under different sediment availabilities and specific gravity. *Journal of Engineering Mechanics* **129**(10): 1206-1219. https://doi.org/10.1061/(ASCE)0733-9399(2003)129:10(1206).

Phillips CB, Hill KM, Paola C, Singer MB, Jerolmack DJ. 2018. Effect of flood hydrograph duration, magnitude, and shape on bed load transport dynamics. *Geophysical Research Letters* **45**: 8264–8271. https://doi.org/10.1029/2018GL078976.

Plate EJ. 1994. The need to consider non-stationary sediment transport. *International Journal of Sediment Research* **9**: 117–123.

Plumb BD, Annable WK, Thompson PJ, Hassan MA. 2017. The impact of urbanization on temporal changes in sediment transport in a gravel-bed channel in Southern Ontario, Canada. *Water Resources Research* **53**: doi:https://doi.org/10.1002/2016WR020288

Poff NL, Allan JD, Bain MB, Karr JR, Prestegaard KL, Richter BD, Sparks RE, Stromberg JC. 1997. The natural flow regime. *Bioscience* **47**(11): 769–784. https://doi.org/10.2307/1313099.

Redolfi M, Bertoldi W, Tubino M, Welber M. 2018. Bed load variability and morphology of gravel bed rivers subject to unsteady flow: a laboratory investigation. *Water Resources Research* **54**(2): 842–862. https://doi.org/10.1002/2017wr021143.

Reid I, Frostick LE, Layman JT. 1985. The incidence and nature of bedload transport during flood flows in coarse-grained alluvial channels. *Earth Surface Processes and Landforms* **10**: 33–44. https://doi.org/10.1002/esp.3290100107.

Richards KS. 1976. The morphology of riffle-pool sequences. *Earth Surface Processes* **1**: 71–88. https://doi.org/10.1002/esp.3290010108.

Schumm S.A., Mosley M.P., & Weaver W.E.. 1987. *Experimental Fluvial Geomorphology*, Wiley: New York 413.

Shields FD, Jr, Cooper CM, Jr, Knight SS, Moore MT. 2003. Stream corridor restoration research: a long and winding road. *Ecological Engineering* **20**(5): 441–454. https://doi.org/10.1016/j.ecoleng.2003.08.005.

Sidle RC. 1988. Bed load transport regime of a small forest stream. *Water Resources Research* **24**(2): 207–218. https://doi.org/10.1029/WR024i002p00207.

Surian N, Mao L, Giacomin M, Ziliani L. 2009. Morphological effects of different channel-forming discharges in a gravel-bed river. *Earth Surface Processes and Landforms* **34**(8): 1093–1107. https://doi.org/10.1002/esp.1798.

Tan L, Curran JC. 2012. Comparison of turbulent flows over clusters of varying density. *Journal of Hydraulic Engineering* **138**(12): 1031–1044.

Thompson PJ. 2013. Event based characterization of hydrologic change in urbanizing southern Ontario watersheds via high resolution stream gauge data. In *American Geophysical Union, Fall Meeting 2011*, abstract id. H52F-03.

Walsh C, Roy A, Feminella J, Cottingham P, Groffman P, Raymond M. 2005. The urban stream syndrome: current knowledge and the search for a cure. *Journal of the North American Benthological Society* **24**: 706–723. https://doi.org/10.1899/0887-3593(2005)024\[0706:TUSSCK\]2.0.CO;2.

Wang L, Cuthbertson AJS, Pender G, Cao Z. 2015. Experimental investigations of graded sediment transport under unsteady flow hydrographs. *International Journal of Sediment Research* **30**(4): 306–320. https://doi.org/10.1016/j.ijsrc.2015.03.010.

Waters KA, Curran JC. 2015. Linking bed morphology changes of two sediment mixtures to sediment transport predictions in unsteady flows. *Water Resources Research* **51**(4): 2724–2741. https://doi.org/10.1002/2014WR016083.

Williams GP. 1989. Sediment concentration versus water discharge during single hydrologic events in rivers. *Journal of Hydrology* **111**(1): 89–106.

Wolman MG, Miller JP. 1960. Magnitude and frequency of forces in geomorphic processes. *Journal of Geology* **68**(1): 54–74. https://doi.org/10.1086/626637.

Yen CL, Lee KT. 1995. Bed topography and sediment sorting in channel bend with unsteady flow. *Journal of Hydraulic Engineering* **121**(8): 591–599.

Zhang X, Zwiers F, Hegerl G, Lambert F, Gillett N, Solomon S, Stott P, Nozawa T. 2007. Detection of human infuence on twentieth-century precipitation trends. *Nature* **448**: 461–465. https://doi.org/10.1038/nature06025.